Quantitative Assessments of Tumor Activity in a General Oncologic PET/CT Population: Which Metric Minimizes Tracer Uptake Time Dependence?

Semra Ince[1], Richard Laforest[1], Malak Itani[1], Vikas Prasad[1], Paul-Robert Derenoncourt[1], John P. Crandall[1], Saeed Ashrafinia[2], Anne M. Smith[2], Richard L. Wahl[1,3], and Tyler J. Fraum[1]

[1]*Department of Radiology, Washington University School of Medicine, St. Louis, Missouri;* [2]*Siemens Medical Solutions Inc., Knoxville, Tennessee; and* [3]*Department of Radiation Oncology, Washington University School of Medicine, St. Louis, Missouri*

In oncologic PET, the SUV and standardized uptake ratio (SUR) of a viable tumor generally increase during the postinjection period. In contrast, the net influx rate (K_i), which is derived from dynamic PET data, should remain relatively constant. Uptake-time-corrected SUV (cSUV) and SUR (cSUR) have been proposed as uptake-time-independent, static alternatives to K_i. Our primary aim was to quantify the intrascan repeatability of K_i, SUV, cSUV, SUR, and cSUR among malignant lesions on PET/CT. An exploratory aim was to assess the ability of cSUR to estimate K_i. **Methods:** This prospective, single-center study enrolled adults undergoing standard-of-care oncologic PET/CT. SUV and K_i images were reconstructed from dynamic PET data obtained before (~35–50 min after injection) and after (~75–90 min after injection) standard-of-care imaging. Tumors were manually segmented. Quantitative metrics were extracted. cSUVs and cSURs were calculated for a 60-min postinjection reference uptake time. The magnitude of the intrascan test–retest percent change (test–retest |%Δ|) was calculated. Coefficients of determination (R^2) and intraclass correlation coefficients (ICC) were also computed. Differences between metrics were assessed via the Wilcoxon signed-rank test (α, 0.05). **Results:** This study enrolled 78 subjects; 41 subjects (mean age, 63.8 y; 24 men) with 116 lesions were analyzed. For both tracers, SUV_{max} and maximum SUR (SUR_{max}) had large early-to-late increases (i.e., poor intrascan repeatability). Among [^{18}F]FDG-avid lesions (n = 93), there were no differences in intrascan repeatability (median test–retest |%Δ|; ICC) between the maximum K_i ($K_{i,max}$) (13%; 0.97) and either the maximum cSUV ($cSUV_{max}$) (12%, P = 0.90; 0.96) or the maximum cSUR ($cSUR_{max}$) (13%, P = 0.67; 0.94). For DOTATATE-avid lesions (n = 23), there were no differences in intrascan repeatability between the $K_{i,max}$ (11%; 0.98) and either the $cSUV_{max}$ (13%, P = 0.41; 0.98) or the $cSUR_{max}$ (11%, P = 0.08; 0.94). The SUV_{max}, $cSUV_{max}$, SUR_{max}, and $cSUR_{max}$ were all strongly correlated with the $K_{i,max}$ for both [^{18}F]FDG (R^2, 0.81–0.92) and DOTATATE (R^2, 0.88–0.96), but the $cSUR_{max}$ provided the best agreement with the $K_{i,max}$ across early-to-late time points for [^{18}F]FDG (ICC, 0.69–0.75) and DOTATATE (ICC, 0.90–0.91). **Conclusion:** $K_{i,max}$, $cSUV_{max}$, and $cSUR_{max}$ had low uptake time dependence compared with SUV_{max} and SUR_{max}. The $K_{i,max}$ can be predicted from $cSUR_{max}$.

Key Words: Patlak slope; PET; corrected SUV; metabolic rate

J Nucl Med 2024; 65:1349–1356
DOI: 10.2967/jnumed.123.266469

In oncologic imaging, SUV changes between scans are critical for treatment response assessment (*1*). However, SUV depends on uptake times, as many tumors accumulate tracer continuously (*2,3*). The logistic demands of busy clinical PET services often preclude precise scan-to-scan reproduction of uptake times, reducing the reliability of SUV as an oncologic biomarker (*4*). The Patlak model, which attempts to ameliorate this shortcoming, assumes that circulating tracer is trapped irreversibly, allowing tracer uptake to be quantified via the net influx rate (K_i) (*5,6*). Several clinically used PET tracers, including [^{18}F]FDG, approximate this behavior, permitting Patlak modeling of dynamic PET data. Once steady-state conditions are achieved between the blood and tissue compartments, the K_i should remain relatively constant, whereas the SUV is expected to increase with time. Furthermore, K_i-based metrics are promising prognostic biomarkers for several cancer types, occasionally outperforming SUV-based metrics (*7,8*).

However, K_i derivation requires direct measurement or estimation of arterial input functions (AIFs) and dynamic acquisitions to generate tissue time–activity curves (*5*). The required modifications to PET protocols may increase imaging time or introduce motion-related quantitative errors (*9*). The uptake-time-corrected SUV (cSUV), which involves retrospectively modifying an observed SUV on the basis of actual versus targeted uptake times, is an alternative means of addressing the uptake time dependence of SUVs (*10*). Furthermore, the uptake-time-corrected tumor-to-blood standardized uptake ratio (cSUR) may allow for K_i estimation, without the need for AIFs or dynamic imaging (*11*).

To our knowledge, no prior studies have assessed the relative temporal stabilities of SUV, SUR, K_i, cSUV, and cSUR in a broad oncologic PET population. Thus, our primary aim was to quantify the intrascan repeatability of these metrics and thereby determine which approach provides the most time-independent assessment of tracer avidity on [^{18}F]FDG PET and DOTATATE PET. An exploratory aim was to determine the ability of cSUR to estimate K_i.

MATERIALS AND METHODS

Study Design

This prospective, Institutional Review Board–approved, Health Insurance Portability and Accountability Act–compliant study (NCT04283552)

Received Jul. 28, 2023; revision accepted Jul. 10, 2024.
For correspondence or reprints, contact Tyler J. Fraum (fraumt@wustl.edu).
Published online Aug. 14, 2024.

enrolled 78 subjects from a pool of consecutive patients scheduled to undergo standard-of-care (SOC) oncologic PET/CT for various indications, using [^{18}F]FDG, [^{68}Ga]Ga-DOTATATE, [^{64}Cu]Cu-DOTATATE, or [^{18}F]piflufolastat (note that [^{68}Ga]Ga-DOTATATE and [^{64}Cu]Cu-DOTATATE are hereafter collectively called DOTATATE, as these scans were analyzed together). These tracers have been reported to satisfy the Patlak model's assumptions (*12–14*). The 2 [^{18}F]piflufolastat studies were excluded because of insufficient cases for tracer-specific analysis. All imaging occurred at a tertiary-care center between June 2020 and October 2022. Inclusion criteria included being at least 18 y of age, having the ability to provide written informed consent, and self-reporting the ability to tolerate approximately 90 min of near-motionless supine positioning. Study imaging was performed before and after SOC PET/CT using the same tracer dose.

Imaging Protocol

The study imaging protocol (details are available in the supplemental materials; available at http://jnm.snmjournals.org) is summarized in Figure 1. All patients were imaged on a single Biograph Vision 600 PET/CT scanner (Siemens Healthineers) equipped with commercially available software for direct reconstruction of multiparametric PET images (FlowMotion Multiparametric PET Suite; Siemens Healthineers).

PET Image Reconstruction

Using automated scanner tools, volumes of interest were placed in the descending thoracic aorta on a 6-min dynamic chest acquisition and the subsequent 10 whole-body (WB) passes (*15*). Per default scanner software settings, AIFs were generated from measured blood activity concentrations via exponential ([^{18}F]FDG) or linear piecewise (DOTATATE) curve fitting. After all WB PET passes were reviewed dynamically for large bulk motion events, early and late SUV and K_i images were reconstructed per manufacturer-recommended parameters (Supplemental Table 1). Each reconstruction used data from three 5-min WB passes with targeted acquisition times of 35–50 min (early) and 75–90 min (late) after injection. Note that the scanner software requires at least 3 WB passes for Patlak analysis. The 3 latest pre-SOC WB passes were selected for the early images, ensuring adequate time to achieve steady-state conditions. Importantly, subjects left the scanner to void immediately before SOC imaging per our standard clinical protocol, precluding automated scanner measurement of post-SOC blood tracer concentrations due to different patient positioning. Consequently, the AIF for the post-SOC K_i reconstructions was automatically derived by the scanner software from extrapolation of the pre-SOC AIF (i.e., no incorporation of measured post-SOC blood tracer concentrations). SUV was based on actual body weight with units of grams per milliliter. K_i had units of milliliter per minute per 100 mL. In contrast to [^{18}F]FDG, intravascular DOTATATE does not enter red blood cells, requiring correction of measured K_i values for the subjects' hematocrit levels (*16*):

$$\text{corrected } K_i = \frac{\text{measured } K_i}{1-\text{hematocrit}}.$$

Quantitative Analysis

Tracer-avid lesions deemed to represent sites of viable malignancy on the SOC PET/CT interpretation were selected by one author. In cases of numerous lesions, the largest or most tracer-avid lesions were selected (5 per subject maximum). Each lesion was manually segmented in MIM version 7.1.5 (MIM Software) on 4 PET image sets (K_i-early, SUV-early, K_i-late, SUV-late) to generate volumes of interest, using coregistered CT images for guidance. Maximum and peak values were extracted. Additionally, a cylindric volume of interest (1-cm diameter, 6-cm length) was placed in the descending thoracic aorta (avoiding vessel walls) to extract a mean value for SUR calculation:

$$\text{tumor SUR} = \frac{\text{tumor SUV}}{\text{blood SUV}}.$$

SUV_{max} and SUV_{peak} were used to calculate maximum SUR (SUR_{max}) and peak SUR (SUR_{peak}), respectively; the SUV_{mean} of blood was used in both cases.

Uptake Time Correction

Actual uptake time ranges were extracted for each image set, with the mid point defining the effective uptake time (e.g., 44.5 min for 37–52 min after injection). cSUV and cSUR were calculated as follows (*10,11*):

$$\text{cSUV} = \text{SUV}\times\left(\frac{T_c}{T_0}\right)^{1-b},$$

$$\text{cSUR} = \text{SUR}\times\left(\frac{T_c}{T_0}\right).$$

SUV and SUR are measured values, T_0 is the actual uptake time, and T_c is the correction time reference. T_c was set to 60 min, reflecting a commonly targeted uptake time in [^{18}F]FDG and DOTATATE

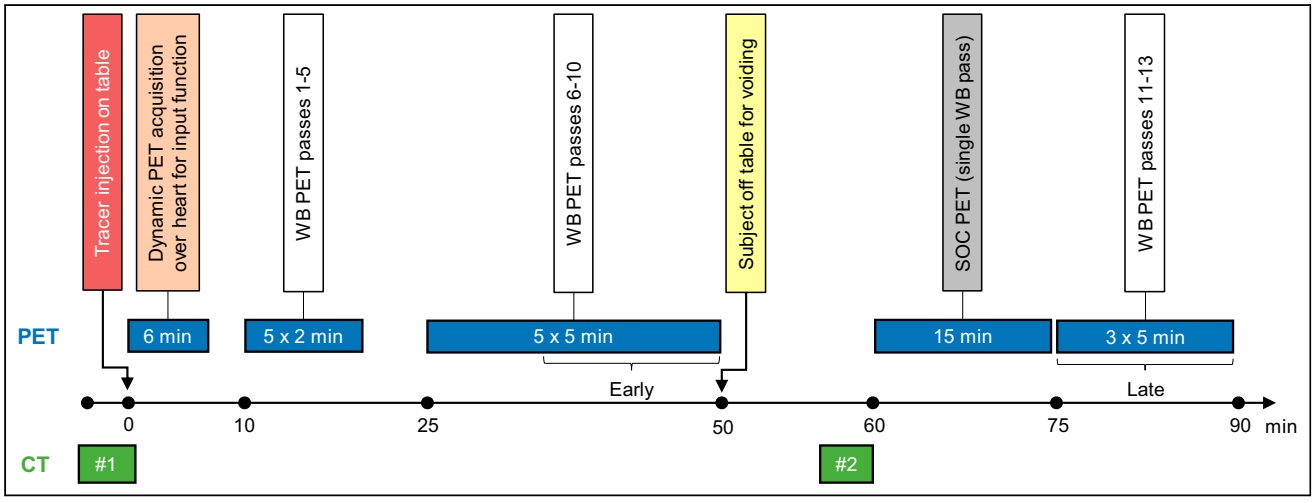

FIGURE 1. PET/CT acquisition protocol. Brackets show timing of data used for early and late image reconstructions.

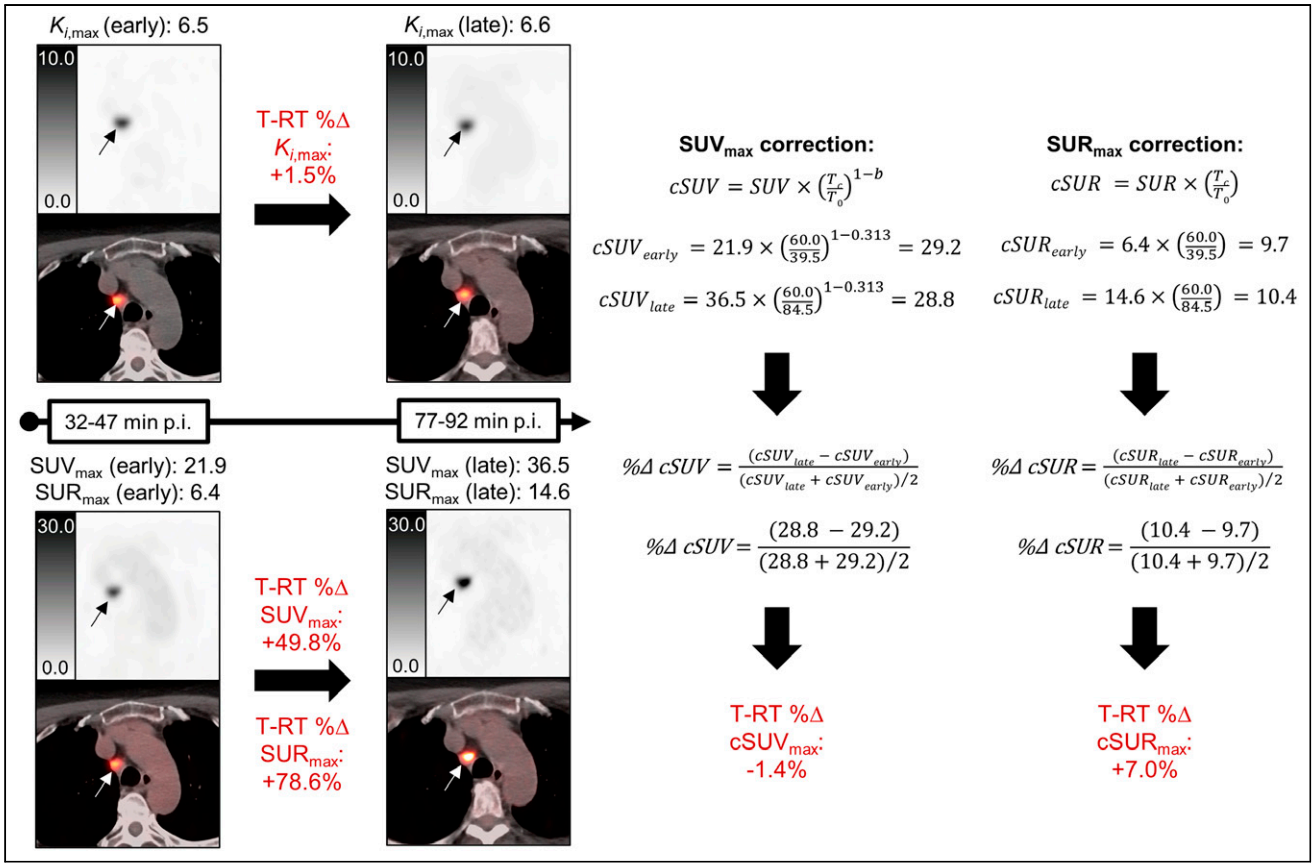

FIGURE 2. Uptake time correction procedure for SUV and SUR. Axial [^{18}F]FDG PET and fused [^{18}F]FDG PET/CT images are shown for K_i (top) and SUV (bottom) reconstructions at early and late time points. $K_{i,max}$, SUV$_{max}$, and SUR$_{max}$ of [^{18}F]FDG-avid mediastinal lymph node (arrows) are shown. Test–retest %Δ values were 1.5%, 49.8%, and 78.6% for $K_{i,max}$, SUV$_{max}$, and SUR$_{max}$, respectively, indicating much better intrascan repeatability for $K_{i,max}$. Procedure for correcting SUV$_{max}$ and SUR$_{max}$ to 60 min after injection is also shown. Test–retest %Δ values were −1.4% for cSUV$_{max}$ and +7.0% for cSUR$_{max}$, similar to $K_{i,max}$ results.

protocols (*1*). Figure 2 shows the SUV and SUR correction procedure for a representative case. For [^{18}F]FDG, the value of the parameter b of 0.313 was based on a prior study (*10*). For DOTATATE, we empirically derived a b of 0.63 by determining the value (averaged across all subjects) that best reproduced the observed late SUV$_{max}$ from the observed early SUV$_{max}$. The early and late values were then corrected to 60 min with the cSUV equation.

Manual Patlak Analysis

To explore apparent temporal variations in K_i, we selected 6 [^{18}F]FDG, 1 [^{68}Ga]Ga-DOTATATE, and 2 [^{64}Cu]Cu-DOTATATE cases with at least 1 lesion exhibiting a large (>20% or <20%) test–retest percent change (%Δ) in maximum K_i ($K_{i,max}$) for further analysis. For all 9 cases, extrapolated AIF curve fits were compared with manually measured blood activity concentrations on the WB passes. Areas under the time–activity curve were compared for extrapolated AIF curve fits versus manual measurements via trapezoidal integration. For 4 cases, full manual Patlak analysis was performed for selected lesions and reference organs (supplemental materials) (*17–20*).

Statistical Analysis

Statistical analysis was conducted in Prism 9 (GraphPad) and Excel 2016 (Microsoft) by one author with statistician guidance. Participant and scan characteristics were summarized descriptively. Because of the anticipated pharmacokinetic differences, the [^{18}F]FDG cases were analyzed separately from the DOTATATE cases. The 2-tailed Wilcoxon signed-rank test was used for pairwise comparisons of quantitative metrics. Intrascan test–retest changes were computed:

$$\text{test-retest } \Delta = \text{late} - \text{early}.$$

To facilitate comparisons across metrics of different magnitudes, intrascan test–retest %Δ was also computed:

$$\text{test-retest } \%\Delta = \frac{\text{late} - \text{early}}{(\text{late} + \text{early})/2}.$$

Results were displayed via Bland–Altman plots and box-and-whisker plots (*21*). The mean (μ) and SD (σ) of the test–retest Δ and test–retest %Δ distributions were determined for each metric. The 95% limits of repeatability were defined as follows:

$$95\%\text{ limits of repeatability} = \mu \pm 2\sigma.$$

Given that near-zero %Δ values could be due to averaging of large negative and positive changes, absolute test–retest %Δ (test–retest |%Δ|) values were also computed. Intraclass correlation coefficients (ICC) and coefficients of determination (R^2) were also used to assess test–retest repeatability and to quantify the accuracy of K_i prediction by other metrics. A P value of less than 0.05 defined statistical significance. More detailed statistical methods are available in the supplemental materials (*22*).

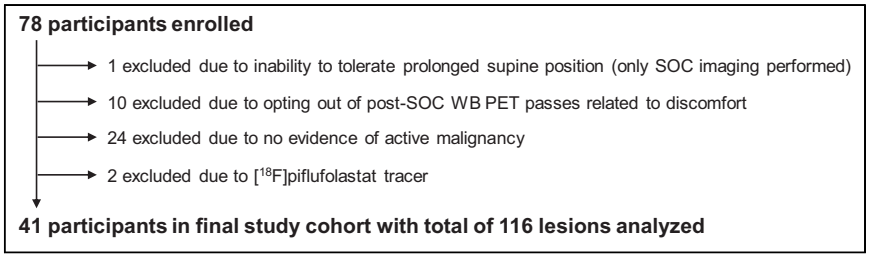

FIGURE 3. Study flowchart.

RESULTS

Study Cohort

Of the 78 study subjects, 41 subjects with 116 lesions (93 on [^{18}F]FDG; 23 on DOTATATE) were included in the analysis (Fig. 3). This study cohort was 58.5% men (24/41) with a mean age of 63.8 y. Additional patient and scan characteristics are captured in Supplemental Table 2.

Intrascan Repeatability of Tumor Uptake Metrics

Test–retest repeatability results are summarized in Table 1 ([^{18}F]FDG) and Supplemental Table 3 (DOTATATE). Scatterplots of late versus early metric values are shown in Supplemental Figures 1 and 2 ([^{18}F]FDG) and Supplemental Figures 3 and 4 (DOTATATE). Bland–Altman plots for K_i, cSUV, and cSUR are displayed in Figure 4 ([^{18}F]FDG) and Supplemental Figure 5 (DOTATATE). Table 2 ([^{18}F]FDG) and Supplemental Table 4 (DOTATATE) summarize test–retest |%Δ| values for all metrics. Box-and-whisker plots of test–retest %Δ and test–retest |%Δ| distributions are presented in Figure 5 ([^{18}F]FDG) and Supplemental Figure 6 (DOTATATE). The remainder of this section focuses on the [^{18}F]FDG results, except as noted (detailed DOTATATE results are provided in the supplemental materials).

As expected, SUV and SUR metrics showed large, statistically significant early-to-late increases. In contrast, cSUV and cSUR metrics were similar at early and late time points, though with some small but significant early-to-late changes. For the maximum cSUV ($cSUV_{max}$), the early and late values were statistically equivalent (median, 8.0 vs. 7.3; $P = 0.17$). Surprisingly, the K_i metrics exhibited significant early-to-late increases (median, 1.8 vs. 2.3; $P < 0.001$). The early and late values of each metric were strongly correlated (R^2, 0.90–0.96). However, the ICCs showed substantially better agreement between early and late values for K_i, cSUV, and cSUR metrics (range, 0.91–0.97) than for SUV and SUR metrics (range, 0.27–0.75). For DOTATATE, the results were similar, except that the K_i metrics exhibited significant (or nearly significant) early-to-late decreases.

In the Bland–Altman analysis, $cSUV_{max}$ and maximum cSUR ($cSUR_{max}$) showed the least bias between early and late values, with mean test–retest %Δ values of −6% and 7%, respectively, compared with 11% for $K_{i,max}$. In contrast, the mean test–retest %Δ values for SUV_{max} and SUR_{max} were 47% and 81%, respectively, indicating large early-to-late increases. Regarding the magnitude of deviation from perfect repeatability (i.e., test–retest $|\%\Delta| = 0$), the test–retest $|\%\Delta|$ of $K_{i,max}$ (median, 13%) was similar to those of $cSUV_{max}$ (median, 12%; $P = 0.90$) and $cSUR_{max}$ (median, 13%; $P = 0.67$) but significantly less than those of SUV_{max} (median, 48%; $P < 0.001$) and SUR_{max} (median, 81%; $P < 0.001$). The test–retest $|\%\Delta|$ of the peak K_i ($K_{i,peak}$) (median, 15%) was significantly lower than that of all other relevant metrics except for the peak cSUR ($cSUR_{peak}$) (median, 13%; $P = 0.36$). For DOTATATE, the results were similar to those of [^{18}F] FDG for the $K_{i,max}$ analysis, though the median test–retest $|\%\Delta|$ of the $K_{i,peak}$ was similar to that of SUV_{peak} (rather than $cSUR_{peak}$).

Prediction of K_i by cSUR

Supplemental Figures 7 and 8 ([^{18}F]FDG) and Supplemental Figures 9 and 10 (DOTATATE) show correlation results for $K_{i,max}$ versus SUV_{max}, SUR_{max}, $cSUV_{max}$, and $cSUR_{max}$. For [^{18}F]FDG, the

TABLE 1
Intrascan Repeatability of SUV, cSUV, SUR, cSUR, and K_i Metrics Among [^{18}F]FDG-Avid Lesions

Metric	Early*	Late*	$P^{\dagger}$	R^2	ICC	T-RT Δ‡	T-RT %Δ‡
$K_{i,max}$ (mL/min/100 mL)	1.8 (1.1, 3.4)	2.3 (1.2, 3.5)	**<0.001**	0.96	0.97	0.2 (−0.6, 1.1)	11% (−32%, 54%)
$K_{i,peak}$ (mL/min/100 mL)	1.2 (0.7, 2.1)	1.4 (0.9, 2.5)	**<0.001**	0.96	0.97	0.2 (−0.4, 0.8)	15% (−30%, 59%)
SUV_{max} (g/mL)	6.0 (3.9, 7.5)	9.2 (5.8, 14.5)	**<0.001**	0.93	0.64	4.9 (−4.9, 14.8)	47% (3%, 91%)
SUV_{peak} (g/mL)	3.8 (2.6, 5.7)	5.2 (2.9, 8.5)	**<0.001**	0.90	0.75	1.9 (−2.9, 6.7)	26% (−22%, 75%)
$cSUV_{max}$ (g/mL)	8.0 (5.2, 10.1)	7.3 (4.4, 11.5)	0.17	0.92	0.96	0.0 (−4.4, 4.4)	−6% (−53%, 41%)
$cSUV_{peak}$ (g/mL)	5.2 (3.5, 7.9)	3.8 (2.2, 6.7)	**<0.001**	0.90	0.91	−1.1 (−3.8, 1.5)	−27% (−77%, 23%)
SUR_{max} (g/mL)	2.1 (1.4, 3.1)	5.1 (3.2, 8.2)	**<0.001**	0.92	0.27	3.8 (−2.0, 9.6)	81% (48%, 114%)
SUR_{peak} (g/mL)	1.4 (1.0, 2.1)	2.8 (1.7, 4.5)	**<0.001**	0.94	0.41	1.8 (−1.4, 5.0)	63% (23%, 102%)
$cSUR_{max}$ (g/mL)	3.2 (2.2, 4.7)	3.4 (2.3, 5.7)	**<0.001**	0.93	0.94	0.5 (−1.4, 2.4)	7% (−33%, 48%)
$cSUR_{peak}$ (g/mL)	2.2 (1.4, 3.1)	1.9 (1.2, 3.3)	**<0.001**	0.94	0.96	−0.2 (−1.1, 0.8)	−14% (−60%, 33%)

*Values are median with first quartile and third quartile in parentheses.
†Early versus late values via Wilcoxon signed-rank test.
‡Values are mean with 95% limits of repeatability in parentheses.
T-RT = test-retest.
Bold *P* values are statistically significant.

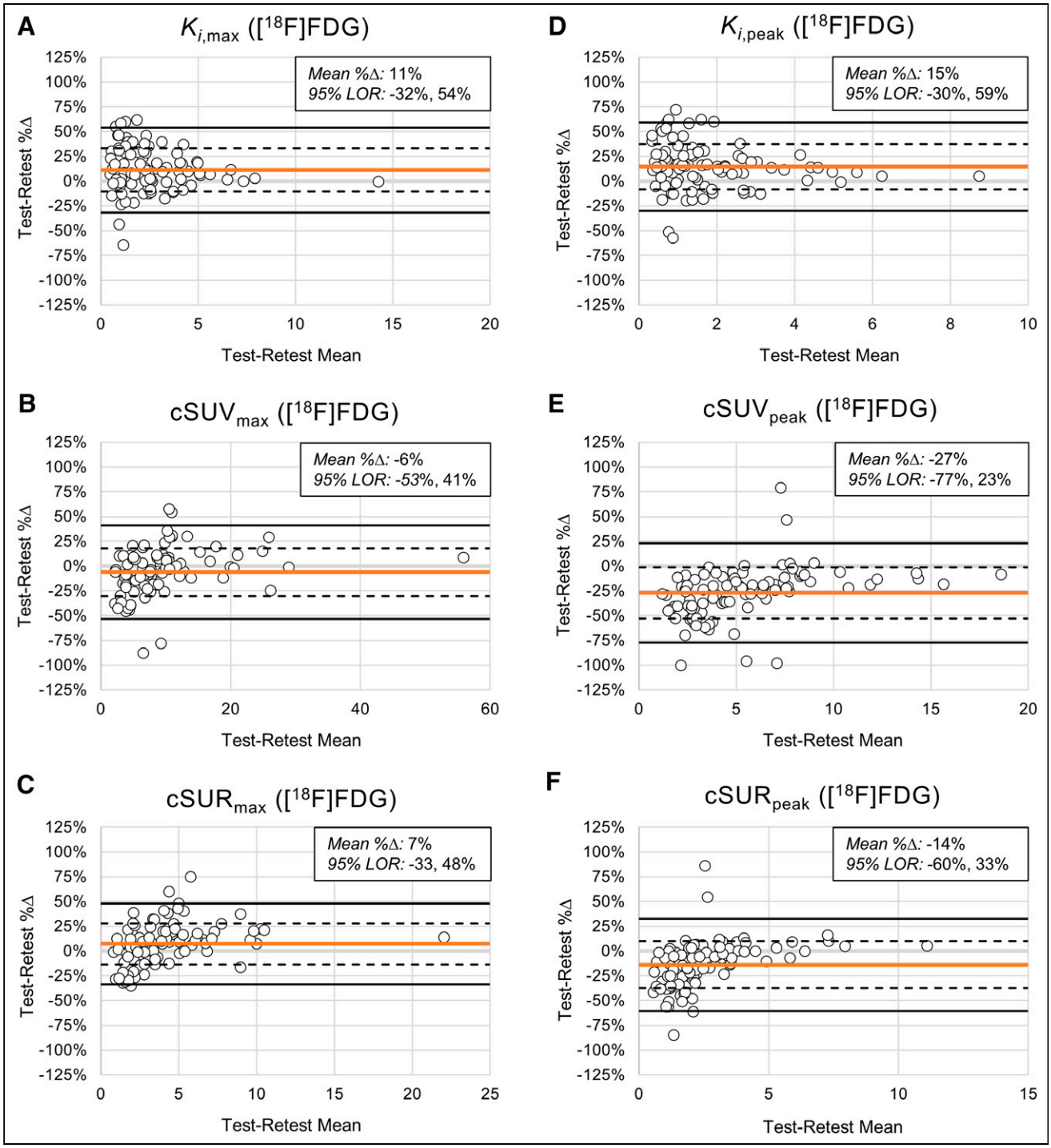

FIGURE 4. Intrascan test–retest repeatability for [^{18}F]FDG-avid lesions. Bland–Altman plots are shown for $K_{i,max}$ (A), $cSUV_{max}$ (B), $cSUR_{max}$ (C), $K_{i,peak}$ (D), $cSUV_{peak}$ (E), and $cSUR_{peak}$ (F). Horizontal orange lines represent test–retest %Δ means. Horizontal dashed and solid black lines represent $\pm 1\sigma$ and $\pm 2\sigma$ for test–retest %Δ distributions, respectively. Each open circle represents [^{18}F]FDG-avid lesion. 95% limits of repeatability (LOR) are computed as -2σ, $+2\sigma$.

maximum values of all 4 metrics strongly predicted the corresponding early (R^2, 0.81–0.92) and late (R^2, 0.81–0.91) $K_{i,max}$ values. However, agreement with $K_{i,max}$ by ICCs was the highest for SUR_{max} (0.94) and $cSUR_{max}$ (0.75) at the early time point and for $cSUR_{max}$ (0.69) at the late time point. Similarly, for DOTATATE, the maximum values of all 4 metrics strongly predicted the corresponding early (R^2, 0.88–0.96) and late (R^2, 0.88–0.93) $K_{i,max}$ values. However, in contrast to [^{18}F]FDG, agreement with $K_{i,max}$ by ICCs was high for all 4 metrics at the early time point (range, 0.85–0.93) but only for $cSUV_{max}$ (0.78) and $cSUR_{max}$ (0.90) at the late time point.

TABLE 2
Test–retest Absolute %Δ for SUV, cSUV, SUR, cSUR, and K_i Metrics Among [^{18}F]FDG-Avid Lesions

Metric	T-RT |%Δ|*	$P^{\dagger}$
$K_{i,max}$	13% (6%, 29%)	*ref*
SUV_{max}	48% (37%, 59%)	**<0.001**
SUR_{max}	81% (73%, 90%)	**<0.001**
$cSUV_{max}$	12% (7%, 26%)	0.90
$cSUR_{max}$	13% (7%, 24%)	0.67
$K_{i,peak}$	15% (11%, 26%)	*ref*
SUV_{peak}	32% (17%, 43%)	**<0.001**
SUR_{peak}	66% (52%, 76%)	**<0.001**
$cSUV_{peak}$	25% (13%, 42%)	**0.004**
$cSUR_{peak}$	13% (6%, 32%)	0.36

*Values are median with first quartile and third quartile in parentheses.

†Comparison to $K_{i,max}$ (rows 1–5) or $K_{i,peak}$ (rows 6–10) via Wilcoxon signed-rank test.

T-RT = test–retest; *ref* = reference.

Bold *P* values are statistically significant.

Manual Patlak Analysis

Supplemental Figures 11 and 12 show $K_{i,max}$ test–retest %Δ values for each subject's lesions for [^{18}F]FDG and DOTATATE, respectively. Supplemental Tables 5 and 6 present manual Patlak analyses for several [^{18}F]FDG and DOTATATE subjects, respectively. Supplemental Figures 13 and 14 capture AIF and tissue-response curves and manual Patlak plots for representative [^{18}F]FDG and DOTATATE cases, respectively. Supplemental Figure 15 illustrates the effects of motion and image noise on K_i and SUV. For [^{18}F]FDG, the AIF curve-fit extrapolation mildly underestimated late blood activity concentrations, contributing to higher late K_i values. Furthermore, motion of small lesions across WB passes contributed to K_i errors that were ameliorated by manual frame-by-frame segmentations. For DOTATATE, the AIF curve-fit extrapolation moderately overestimated late blood activity concentrations, resulting in lower late K_i values; additionally, DOTATATE binding appeared to be reversible at late time points for some cases. More details are provided in the supplemental materials.

DISCUSSION

In this study, we quantified the intrascan repeatability of K_i, SUV, cSUV, SUR, and cSUR metrics for [^{18}F]FDG-avid and DOTATATE-avid lesions on WB PET in a general oncology population. For both tracers, SUV_{max} and SUR_{max} showed large early-to-late increases (i.e., poor intrascan repeatability). For [^{18}F]FDG, there were no significant differences in intrascan repeatability between $K_{i,max}$ (median test–retest |%Δ|, 13%; ICC, 0.97) and either $cSUV_{max}$ (median test–retest |%Δ|, 12%; $P = 0.90$; ICC, 0.96) or $cSUR_{max}$ (median test–retest |%Δ|, 13%; $P = 0.67$; ICC, 0.94). The intrascan repeatability of the $K_{i,peak}$ was better than that of the peak cSUV ($cSUV_{peak}$) but similar to that of $cSUR_{peak}$. For DOTATATE, there were no significant differences in intrascan repeatability between $K_{i,max}$ (median test–retest |%Δ|, 11%; ICC, 0.98) and either $cSUV_{max}$ (median test–retest |%Δ|, 13%; $P = 0.41$; ICC, 0.98) or $cSUR_{max}$ (median test–retest |%Δ|, 11%; $P = 0.08$; ICC, 0.94). Again, intrascan repeatability of the $K_{i,peak}$ was better than that of $cSUV_{peak}$ or $cSUR_{peak}$.

Early-to-late increases are a well-known limitation of SUVs and SURs for tumor response assessments (*2,3,23*). As such, the Quantitative Imaging Biomarkers Alliance recommends that uptake times for baseline and follow-up scans be approximately 60 min with a no more than 10 min difference between scans (*1*). However, differences greater than 10 min are not uncommon. Methods to correct SUV and SUR for uptake time (i.e., cSUV, cSUR) have been published (*10,23*). For example, a study reported that correcting SUVs and SURs from 20 min to 55 min after injection reduced differences with actual values at 55 min from −30% to 2% for SUV and from −52% to −3% for SUR (*10*). This study, which used data from 9 male patients with colorectal liver metastases, proposed the simple SUV and SUR correction equations used in our work.

We verified that cSUV, using the published time parameter *b* of 0.313, is a relatively time-independent marker of tumoral [^{18}F]FDG avidity. For [^{18}F]FDG, our mean test–retest %Δ values of −6% and 7% for $cSUV_{max}$ and $cSUR_{max}$, respectively, are slightly greater in magnitude than the values cited above, possibly because of our longer early-to-late intervals or heterogeneous patient cohort. We empirically derived a *b* value of 0.63 for DOTATATE and found that cSUV is also a relatively time-independent marker of tumoral DOTATATE avidity, with mean test–retest %Δ values of 2% and −7% for $cSUV_{max}$ and $cSUR_{max}$, respectively. Compared with $cSUV_{max}$ and $cSUR_{max}$, $cSUV_{peak}$ and $cSUR_{peak}$ showed worse intrascan repeatability, with sizeable negative test–retest %Δ values for both tracers. The reason for this somewhat surprising finding is unclear, as peak measurements (because of their larger sampling volumes and lower potential for noise-related errors) are generally considered more repeatable than maximum measurements (*24*).

In terms of test–retest |%Δ| and ICC, the intrascan repeatability was similar across $K_{i,max}$, $cSUV_{max}$, and $cSUR_{max}$ for both tracers. However, we observed small but statistically significant early-to-late increases and decreases in $K_{i,max}$ for [^{18}F]FDG and DOTATATE cases, respectively. In contrast, $cSUV_{max}$ and $cSUR_{max}$ showed no significant early-to-late changes for either tracer, with the exception of a small significant increase in $cSUR_{max}$ for DOTATATE. For both tracers, the observed early-to-late K_i changes were partially attributable to inaccurate AIF curve-fit extrapolations, the need for which arose from incorporating SOC imaging into our study design. A protocol using nonextrapolated image-derived AIFs or population-based AIFs might reduce these apparent temporal changes in K_i. Several cases suggested late reversibility of DOTATATE binding, also contributing to the observed early-to-late K_i decreases. Overall, $cSUV_{max}$ and $cSUR_{max}$ provided intrascan repeatability similar to that of $K_{i,max}$, without dynamic imaging or AIF estimation.

K_i images may still be worth their inherent complexities, as K_i metrics appear useful for guiding treatment decisions and predicting oncologic outcomes (*7,8,25,26*). One study showed that K_i correlated with SUR (R^2, 0.96) much more strongly than with SUV (R^2, 0.37), with all metrics measured at 50–60 min after injection (*11*). In contrast, we found that SUV_{max}, $cSUV_{max}$, SUR_{max}, and $cSUR_{max}$ all strongly correlated with $K_{i,max}$ for both [^{18}F]FDG (R^2, 0.81–0.92) and DOTATATE (R^2, 0.88–0.96), though $cSUR_{max}$ had the best agreement with $K_{i,max}$ across early and late time points for [^{18}F]FDG (ICC, 0.69–0.75) and DOTATATE (ICC, 0.90–0.91). Our findings

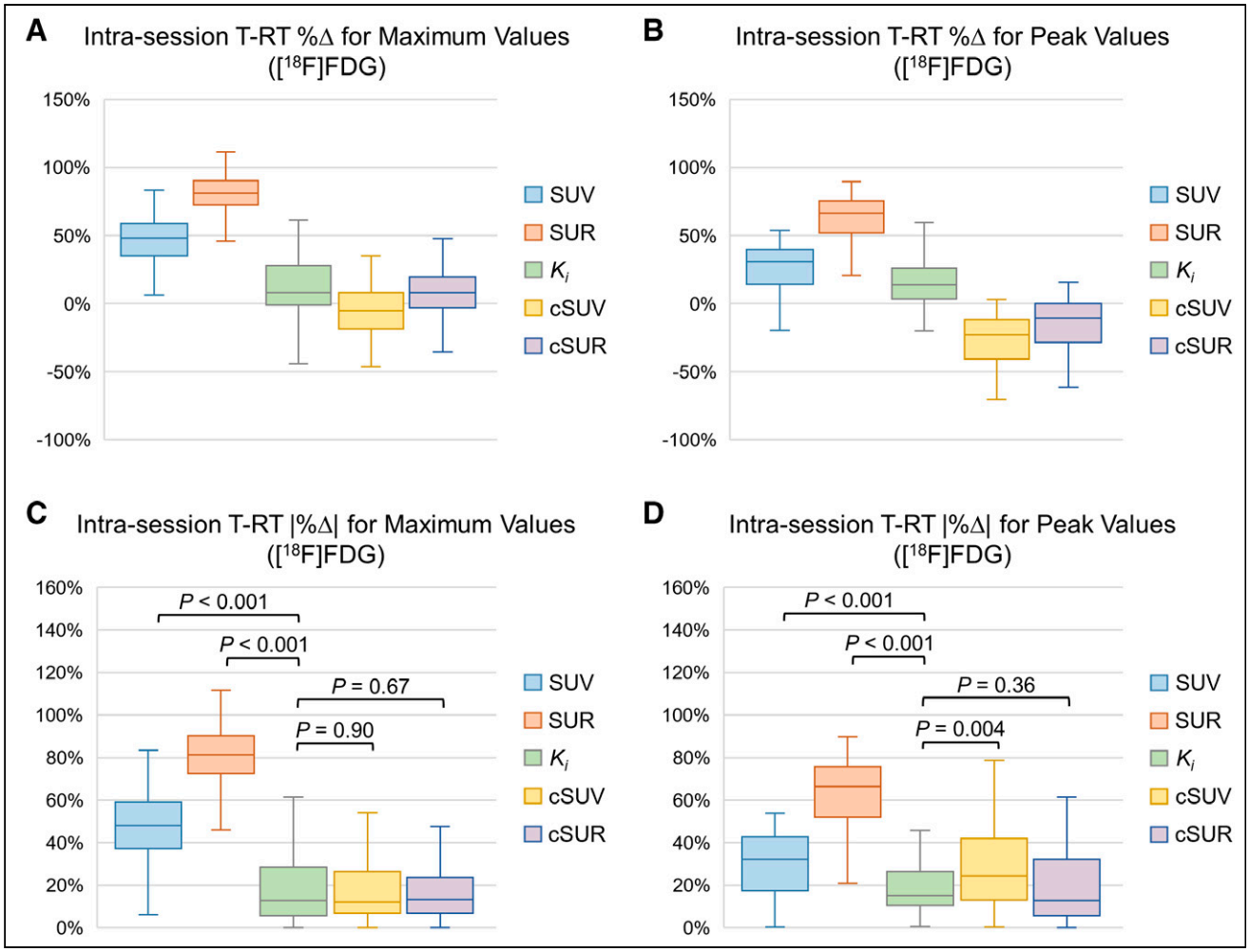

FIGURE 5. Test–retest %Δ and |%Δ| distributions for [^{18}F]FDG-avid lesions. Box-and-whisker plots show test–retest %Δ (A and B) and |%Δ| (C and D) distributions for maximum (A and C) and peak (B and D) values of K_i, SUV, cSUV, SUR, and cSUR. All *P* values are based on comparison to $K_{i,max}$ or $K_{i,peak}$. Table 2 provides descriptive statistics.

indicate that K_i can be predicted from cSUR and that $cSUR_{max}$ exhibits a nearly 1:1 proportionality to $K_{i,max}$. To this point, cSUR and K_i appear to predict postchemoradiation lung cancer outcomes better than does SUV (*27*). That said, Patlak images may provide higher lesion conspicuity and fewer false positives than with SUV images (*28,29*).

Our study has limitations, including its single-center, single-scanner design. The results should be corroborated at other centers on other scanners. Our patient cohort was heterogeneous; the relatively small sample size precluded subgroup analysis by cancer type or imaging indication. The *b* parameter of 0.63 for DOTATATE was derived empirically (rather than from AIF curve fitting) and needs to be validated in other cohorts. Again, the AIF curve-fit extrapolations created late K_i errors. A more thorough investigation of potential causes of the observed temporal variability in K_i is still warranted. Finally, our study excluded subjects who anticipated difficulty with a 90-min imaging period, potentially enriching our cohort for patients capable of remaining relatively motionless; as such, K_i images may be more degraded by motion in an unselected oncologic population.

CONCLUSION

$K_{i,max}$, $cSUV_{max}$, and $cSUR_{max}$ exhibit comparably high intrascan repeatability in a general oncologic population undergoing PET with [^{18}F]FDG or DOTATATE, with significantly less uptake time dependence compared with SUV_{max} and SUR_{max}. $cSUR_{max}$ can predict $K_{i,max}$ without dynamic acquisitions.

DISCLOSURE

This work was supported by a research grant from Siemens Healthineers to Washington University, including salary support for Tyler Fraum. Richard Wahl has received consulting income from Siemens Healthineers. All participants were imaged on a Siemens PET/CT scanner. Saeed Ashrafinia and Anne Smith are Siemens employees. These authors participated in the initial study design, provided occasional technical support, and critically reviewed the manuscript. However, all data collection, analysis, and manuscript preparation were performed by Washington University authors. No other potential conflict of interest relevant to this article was reported.

KEY POINTS

QUESTION: In oncologic PET, which quantitative metric of tracer avidity is least dependent on uptake times?

PERTINENT FINDINGS: In this prospective, cross-sectional study of general oncology subjects undergoing PET with [^{18}F]FDG or DOTATATE, $K_{i,max}$, $cSUV_{max}$, and $cSUR_{max}$ exhibited comparably high intrascan repeatability, whereas SUV_{max} and SUR_{max} substantially increased at later uptake times.

IMPLICATIONS FOR PATIENT CARE: Tracer-avidity metrics with high intrascan repeatability should be used to avoid quantitative interpretive errors related to different uptake times across scans.

REFERENCES

1. Kinahan PE, Perlman ES, Sunderland JJ, et al. The QIBA profile for FDG PET/CT as an imaging biomarker measuring response to cancer therapy. *Radiology.* 2020; 294:647–657.
2. Beaulieu S, Kinahan P, Tseng J, et al. SUV varies with time after injection in ^{18}F-FDG PET of breast cancer: characterization and method to adjust for time differences. *J Nucl Med.* 2003;44:1044–1050.
3. Kramer GM, Frings V, Hoetjes N, et al. Repeatability of quantitative whole-body ^{18}F-FDG PET/CT uptake measures as function of uptake interval and lesion selection in non–small cell lung cancer patients. *J Nucl Med.* 2016;57:1343–1349.
4. Binns DS, Pirzkall A, Yu W, et al. Compliance with PET acquisition protocols for therapeutic monitoring of erlotinib therapy in an international trial for patients with non-small cell lung cancer. *Eur J Nucl Med Mol Imaging.* 2011;38:642–650.
5. Rahmim A, Lodge MA, Karakatsanis NA, et al. Dynamic whole-body PET imaging: principles, potentials and applications. *Eur J Nucl Med Mol Imaging.* 2019;46: 501–518.
6. Patlak CS, Blasberg RG. Graphical evaluation of blood-to-brain transfer constants from multiple-time uptake data: generalizations. *J Cereb Blood Flow Metab.* 1985; 5:584–590.
7. Yin J, Wang H, Zhu G, Chen N, Khan MI, Zhao Y. Prognostic value of whole-body dynamic ^{18}F-FDG PET/CT Patlak in diffuse large B-cell lymphoma. *Heliyon.* 2023;9:e19749.
8. Wang D, Qiu B, Liu Q, et al. Patlak-Ki derived from ultra-high sensitivity dynamic total body [^{18}F]FDG PET/CT correlates with the response to induction immunochemotherapy in locally advanced non-small cell lung cancer patients. *Eur J Nucl Med Mol Imaging.* 2023;50:3400–3413.
9. Sun T, Wu Y, Wei W, et al. Motion correction and its impact on quantification in dynamic total-body ^{18}F-fluorodeoxyglucose PET. *EJNMMI Phys.* 2022;9:62.
10. van den Hoff J, Lougovski A, Schramm G, et al. Correction of scan time dependence of standard uptake values in oncological PET. *EJNMMI Res.* 2014;4:18.
11. van den Hoff J, Oehme L, Schramm G, et al. The PET-derived tumor-to-blood standard uptake ratio (SUR) is superior to tumor SUV as a surrogate parameter of the metabolic rate of FDG. *EJNMMI Res.* 2013;3:77.
12. Gallagher BM, Fowler JS, Gutterson NI, MacGregor RR, Wan CN, Wolf AP. Metabolic trapping as a principle of radiopharmaceutical design: some factors responsible for the biodistribution of [^{18}F] 2-deoxy-2-fluoro-D-glucose. *J Nucl Med.* 1978;19:1154–1161.
13. Lu M, Lindenberg L, Mena E, et al. A pilot study of dynamic ^{18}F-DCFPyL PET/CT imaging of prostate adenocarcinoma in high-risk primary prostate cancer patients. *Mol Imaging Biol.* 2022;24:444–452.
14. Ilan E, Sandström M, Velikyan I, Sundin A, Eriksson B, Lubberink M. Parametric net influx rate images of ^{68}Ga-DOTATOC and ^{68}Ga-DOTATATE: quantitative accuracy and improved image contrast. *J Nucl Med.* 2017;58:744–749.
15. Tao Y, Peng Z, Krishnan A, Zhou XS. Robust learning-based parsing and annotation of medical radiographs. *IEEE Trans Med Imaging.* 2011;30:338–350.
16. Velikyan I, Sundin A, Sörensen J, et al. Quantitative and qualitative intrapatient comparison of ^{68}Ga-DOTATOC and ^{68}Ga-DOTATATE: net uptake rate for accurate quantification. *J Nucl Med.* 2014;55:204–210.
17. Lodge MA, Chaudhry MA, Wahl RL. Noise considerations for PET quantification using maximum and peak standardized uptake value. *J Nucl Med.* 2012;53: 1041–1047.
18. Panin VY, Bal H, Defrise M, Casey ME, Karakatsanis NA, Rahmim A. Whole body parametric imaging on clinical scanner: direct 4D reconstruction with simultaneous attenuation estimation and time-dependent normalization. Presented at: 2015 IEEE Nuclear Science Symposium and Medical Imaging Conference (NSS/MIC); October 31–November 7, 2015; San Diego, CA.
19. Kuwabara H, Gjedde A. Measurements of glucose phosphorylation with FDG and PET are not reduced by dephosphorylation of FDG-6-phosphate. *J Nucl Med.* 1991;32:692–698.
20. Sarikaya I, Sarikaya A, Alnafisi N, Alenezi S. Significance of splenic uptake on somatostatin receptor imaging studies. *Nucl Med Rev Cent East Eur.* 2018;21:66–70.
21. Giavarina D. Understanding Bland Altman analysis. *Biochem Med (Zagreb).* 2015; 25:141–151.
22. Cook RJ, Farewell VT. Multiplicity considerations in the design and analysis of clinical trials. *J R Stat Soc Ser A Stat Soc.* 1996;159:93–110.
23. Hofheinz F, Bütof R, Apostolova I, et al. An investigation of the relation between tumor-to-liver ratio (TLR) and tumor-to-blood standard uptake ratio (SUR) in oncological FDG PET. *EJNMMI Res.* 2016;6:19.
24. Lodge MA. Repeatability of SUV in oncologic ^{18}F-FDG PET. *J Nucl Med.* 2017; 58:523–532.
25. Apostolopoulos DJ, Dimitrakopoulou-Strauss A, Hohenberger P, Roumia S, Strauss LG. Parametric images via dynamic ^{18}F-fluorodeoxyglucose positron emission tomographic data acquisition in predicting midterm outcome of liver metastases secondary to gastrointestinal stromal tumours. *Eur J Nucl Med Mol Imaging.* 2011;38:1212–1223.
26. Cheebsumon P, Velasquez LM, Hoekstra CJ, et al. Measuring response to therapy using FDG PET: semi-quantitative and full kinetic analysis. *Eur J Nucl Med Mol Imaging.* 2011;38:832–842.
27. Hofheinz F, van den Hoff J, Steffen IG, et al. Comparative evaluation of SUV, tumor-to-blood standard uptake ratio (SUR), and dual time point measurements for assessment of the metabolic uptake rate in FDG PET. *EJNMMI Res.* 2016;6:53.
28. Dias AH, Pedersen MF, Danielsen H, Munk OL, Gormsen LC. Clinical feasibility and impact of fully automated multiparametric PET imaging using direct Patlak reconstruction: evaluation of 103 dynamic whole-body ^{18}F-FDG PET/CT scans. *Eur J Nucl Med Mol Imaging.* 2021;48:954.
29. Fahrni G, Karakatsanis NA, Di Domenicantonio G, Garibotto V, Zaidi H. Does whole-body Patlak ^{18}F-FDG PET imaging improve lesion detectability in clinical oncology? *Eur Radiol.* 2019;29:4812–4821.